EPR, FTIR and Raman spectroscopic characterization of Indium barium borate glasses containing Manganese ions

Bodige Narsimha[1], K. Chandrasekhar[1], Md. Shareefuddin[1,] and G. Ramadevudu[2*]

[1]Department of Physics, Osmania University, Hyderabad, India-500007
[2]Department of Physics, Vasavi College of Engineering, Hyderabad, India-500031
[*]Corresponding author email: dr.ramdev@vce.ac.in

Abstract
The impact of indium ions on physical, optical and EPR parameters of Barium borate glass systems comprising manganese ions were examined. The melt quenching method was used to produce $(30-x)BaO-69.5B_2O_3-xIn_2O_3:0.5MnO_2$ (x= 0.5 to 2.5 mol%) glass systems. The amorphous nature of glass samples was validated by X-ray diffraction. Indium oxide incorporation caused nonlinear variation in the physical properties with the increase of In_2O_3 mole%. Optical energy band gap and Urbach energy values estimated from optical absorption. The Mn^{2+} centres in octahedral symmetry were responsible for the six-line hyperfine structure (HF) in EPR spectra. The EPR peaks at g= 3.3 and 4.3 were ascribed to rhombic surroundings manganese ions. A negative shift in g-values is assigned to high ionic region around Mn^{2+} ion in the glass matrix. The hyper fine splitting factor (A) is employed to estimate ionic bonding between the adjoining oxygen ions and Mn^{2+} ions. The total number of spins participated, and susceptibility values are calculated from electron paramagnetic resonance spectra.
Keywords: *Barium Borate glasses; FTIR; EPR; Optical absorption spectrum.*

I. Introduction

Optical materials with high transparency are in greater demand in everyday life due to their use in optical fiber and radiation shielding-related industries. For optically transparent materials, several studies have been undertaken on oxide glasses such as tellurites, phosphates, silicates, and borates. Among all the glass materials, Borate glasses have been extensively explored because of their fascinating special glass network and optical characteristics such as good optical transparency, mechanical strength, chemical and thermal resistance, and ease of strong solubility of rare earth ions [1]. Potential applications for borate glasses include host materials for lasers, optoelectronic components, displays, LED, and transducers etc. The structure of borate glass is complex consisting of BO_3 triangular units, BO_4 tetrahedral units, di-, tri-, and tetraborate groupings. Several dopants are tested to boost the properties of borate oxide glasses. Indium oxide (In_2O_3) possesses a wide band gap, excellent transparency, chemical stability, and electrical conductivity. It is used in electrical, photovoltaic, and optoelectronic devices including gas sensors [2]. The Incorporation of In_2O_3 to $BaO-B_2O_3$ glasses is anticipated to result in fascinating changes in physical, optical, electrical properties, transference, and semi-conducting properties [3].

The present work reports findings of physical, optical, EPR, FTIR, and Raman spectroscopic investigations of manganese ions in $(30-x)$ $BaO-69.5B_2O_3-$ x ln_2O_3 :$0.5MnO_2$ glasses. It is observed that Mn^{2+} ions disperse in $BaO-B_2O_3$ glasses containing In_2O_3. The integration of dopants may expand their optoelectronic applications.

II. Experimental Procedure

In the present study, manganese-doped Indium-barium borate glasses (x = 0.5 to 2.5 mol%) (Table 1) are fabricated by using typical melt quenching approach. BaO and In_2O_3 were systematically varied in the glass matrix, whereas B_2O_3 and MnO mole% remains constant. According to the compositional formula, the stipulated chemicals were weighed using digital balance (Shimazdu). Various components taken in appropriate mole % are placed in crucibles. The mixtures are heated using electric furnace at about 1080° C for 30 minutes, and then the melt is frozen immediately on a preheated steel plate to generate roughly one-millimetre-thick glass samples. In addition, these manufactured glasses are annealed to eliminate any tensions.

Glass samples are subjected to X-ray diffraction (XRD) tests with a Philips Pan analytical X'pert PRO XRD model with Cu-K radiation in two temperature ranges of 10°-80°C in continuous scan mode at ambient temperature. Archimedes' method using Xylene as the immersion liquid is used to estimate the density of BBIM glasses at ambient temperature. Using a Shimadzu UV-1800 spectrometer, the UV-visible optical absorption is measured on glass samples in 190 to 1100 nm wavenumber range at room temperature (RT). The EPR spectra are measured on a BRUKER EPR spectrometer operating at an X-band frequency with modulating frequency 100 kHz in the magnetic field between 2500 and 4000 G. Fourier transform infrared spectra scanned in the wavenumber between 400 and 1600 cm^{-1} using Shimadzu 8400S FTIR spectrometer.

Table1: Composition of xIn_2O_3-$(30-x)BaO$-$69.5B_2O_3$-$0.5MnO$ glasses in mole%

Glass Code	In_2O_3	BaO	B_2O_3	MnO
BBIM-1	0.5	29.5	69.5	0.5
BBIM-2	1.0	29.0	69.5	0.5
BBIM3	1.5	28.5	69.5	0.5
BBIM-4	2.0	28.0	69.5	0.5
BBIM-5	2.5	27.5	69.5	0.5

III. Results and Discussions

3.1 XRD
The X-Ray Diffraction (XRD) patterns of glass systems are depicted fig.1. No noticeable peaks in the diffraction patterns suggested amorphous characteristics of the glass samples.
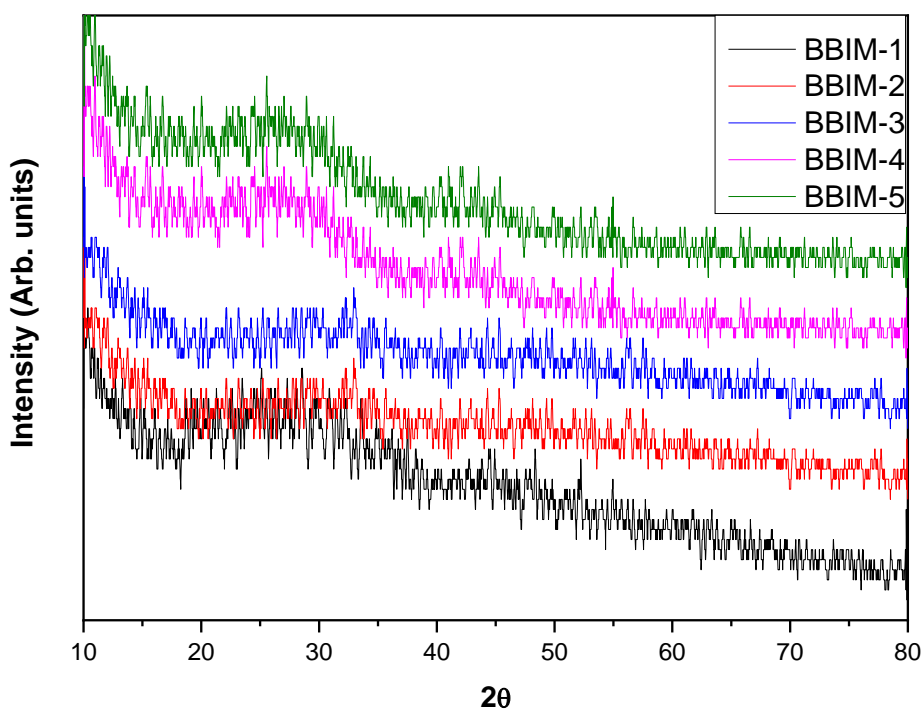
Fig.1. X-ray diffraction patterns of BBIM glass system

3.2. Physical Properties
Density is one of the critical physical parameters used for studying mechanical strength, durability and internal composition. It relates to structural flexibility, geometric alignment, network linkage density, and interstitial space proportions. The density (ρ) values (Table.1) are computed by using the Archimedes method [4]:

$$\rho = \left(\frac{W_p}{W_p - W_q}\right) * 0.86 \qquad (1)$$

Where 'W$_p$' and 'W$_q$' indicates the sample weights in air and xylene, respectively. Density of xylene (density=0.86g/cc). In the present glass system, the density of the BBIM glass system increased non-linearly with increasing indium oxide quantity since the crystalline density of BaO (5.72g/cm^3) is low in comparison to that of In_2O_3 (7.18g/cm^3).

The molar volume (V_m) of each sample is calculated using the formula $V_m = M/\rho$, where M and ρ represents the average molecular weight and density, respectively. V_m values have demonstrated an opposite tendency compared to densities. The observed density (ρ) and computed molar volume (V_m) values are listed in Table 2.

Oxygen Packing Densities are calculated by the formula, OPD= (N/V_m) x1000. Here N represents number of transition metal ions per cubic centimetre. The calculated values of number of TM ions per cubic centimeter, inter molecular distance, polaron radius are mentioned in Table.1. The calculated polaron radii are comparatively modest with respect to the inter ionic distances confirming polaron theory.

3.3. Optical absorption spectra

The optical absorption spectroscopic patterns of BBIM glasses are illustrated in Fig.2.The absorption coefficient (α) is one of the key parameters for the estimation of parameters such as optical energy bandgap, Urbach energy, etc. The absorption coefficient is approximated using absorbance A and thickness of the samples 't' using the relationship given below [5]:

$$\alpha(v) = 2.303 * \frac{A}{t} \qquad (2)$$

The optical energy bandgap of amorphous materials like glasses could be related to absorption coefficient (α) and incident photon energy (hv) as:

$$(\alpha hv) = B \exp(hv - E_{Opt})^n \qquad (3)$$

The optical transitions accepted for glasses as suggested by Tauc [6] for exponent 'n =2', belongs to indirect allowed type transitions. A Tauc plot is drawn between hv and optical energy $(\alpha hv)^{1/2}$. The optical bandgap values are estimated from tangent drawn at the linear section of the curve and extrapolating it to the x-axis as shown in Fig.3.

With growing In_2O_3 mole%, the optical band gap values decreased from 3.132 eV to 3.0350 eV (except BBIM-3). This drop indicates structural changes occurring in the glass. Variation in band gap is often attributable to the formation of bridging oxygens (BOs) and non-bridging oxygens (NBOs). Incorporating In_2O_3 into borate glasses may increase the formation of NBOs, which may then lead to a drop in band gap values.

Table.2. *Physical and optical parameters of the BBIC glass system.*

GLASS CODE	BBIM-1	BBIM-2	BBIM-3	BBIM-4	BBIM-5
Avg. molecular weight	145.982	146.383	146.785	147.186	147.588
Density (ρ-g/cc)	3.69	3.67	3.69	3.73	3.61
Molar volume (V_m)	39.5	39.87	39.78	39.46	40.92
Optical energy band gap (E_g-eV)	3.132	3.107	3.148	3.085	3.053
Urbach Energy (ΔE-eV)	0.253	0.285	0.260	0.310	0.239
Wavenumber (ΔE_{xy} - cm^{-1})	21209	21349	21249	21322	21612
Refractive Index (n)	2.36	2.37	2.36	2.37	2.38
Dielectric Constant (ε)	5.58	5.61	5.56	5.64	5.68
No. of oxygen atoms ($N_O{}^{2-}$)	2.41	2.42	2.43	2.44	2.45
Oxygen packing density (OPD-g-atom litre^{-1})	60.85	60.58	60.96	61.70	59.75
Molar refraction (R_m-cm^3/mol)	23.88	24.15	23.99	23.96	24.93
Reflection loss	0.164	0.165	0.164	0.166	0.167
Molar polarizability α_m (x10^{-24} cm^3)	9.47	9.57	9.51	9.49	9.88
Inter ionic distance (A^o)	18.72	18.77	18.76	18.71	18.94
Polaron radius (r_p)A^o	07.54	07.56	07.56	07.54	07.63
Field Strength(F) (x10^{14}cm^{-2})	3.515	3.495	3.500	3.518	3.434
Molar polarizability (α_m)	0.4826	0.4813	0.4799	0.4786	0.4772
Electronic polarizability of oxide ion (α_0^{2-})	3.740	3.769	3.729	3.709	3.851
Theoretical optical basicity (Λ_{th})	1.264	1.274	1.284	1.294	1.304
Experimental optical basicity (Λ)	1.223	1.227	1.222	1.220	1.236
Interaction Parameter (A_{th})	0.1713	0.1714	0.1716	0.1718	0.1720
Metallization criterion(M)	0.396	0.394	0.397	0.393	0.391
Average boron-boron separation ($d_{b—b}$)	4.730	4.744	4.741	4.728	4.785
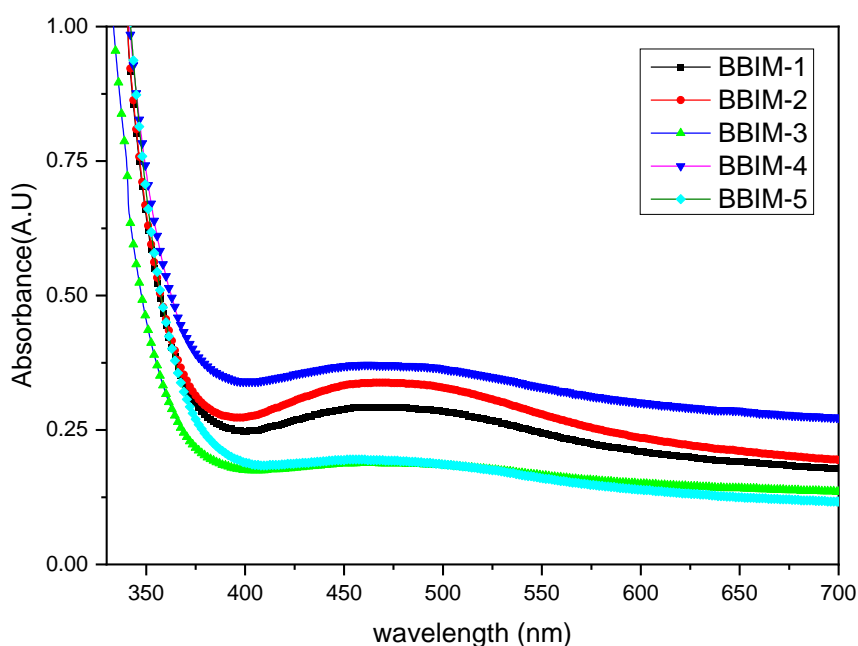
Fig. 2. Optical absorption spectra of BBIM glass system
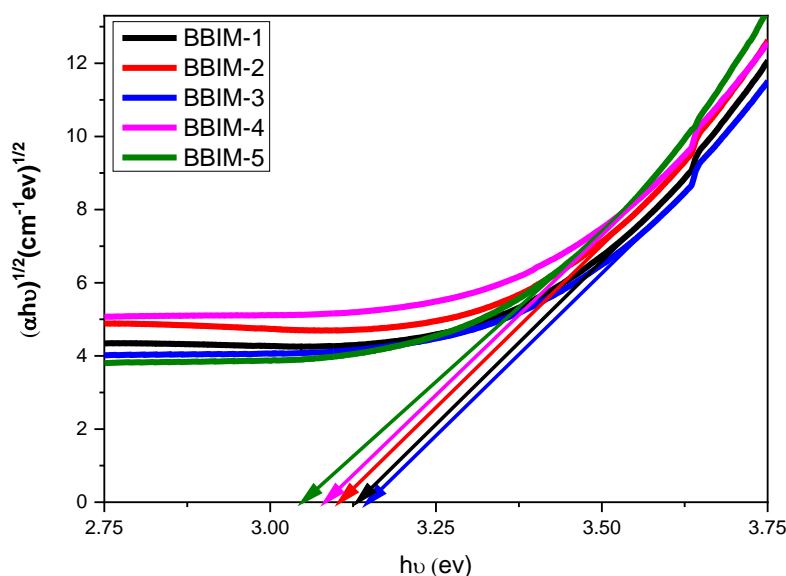
Fig. 3. Tauc plots of BBIM glass system.

With growing In_2O_3 mole%, the optical band gap values decreased from 3.132 eV to 3.0350 eV (except BBIM-3). This drop indicates structural changes occurring in the glass samples. Variation in bandgap is often attributable to formation of bridging oxygens (BOs) and non-bridging oxygens (NBOs). Incorporating In_2O_3 into borate glasses may increase the formation of NBOs, which may then lead to a drop in band gap values.

Urbach energies (ΔE) are computed with the help of the graph draw between $h\upsilon$ and $\ln(\alpha)$ and noting inverse of slope at the linear portion of the Urbach curve [6,7]. The Urbach energies are found to lie between 0.239 and 0.310 eV. It was found that with growing In_2O_3 concentrations, Urbach energy values exhibited nonlinear changes. The low Urbach energy values indicates that the glasses have fewer defects.

Molar polarizabilities (α_m), refractive index (n), molar refraction (R_m) etc., are calculated from optical energy bandgaps and molar volume values through relative formula as proposed by Dimitrov and Sakka [8,9].

In materials containing oxides, the polarizability of the oxide ions is evaluated by using   Lorentz-Lorentz equation [10,11]

$$\alpha_o^{2-}(n) = \left[\frac{R_m}{2.52} - \Sigma\alpha_i\right](N_{o^{2-}})^{-1} \qquad (4)$$

here $\Sigma\alpha_i$ indicates molar cation polarizability. Dimitrov proposed values for $\alpha_{Ba+=}$1.595 for Ba+, $\alpha_{In+} = 0.662$ for In+, α_{Cu+}=0.437 for Cu+, α_{B+}=0.002 for B+.
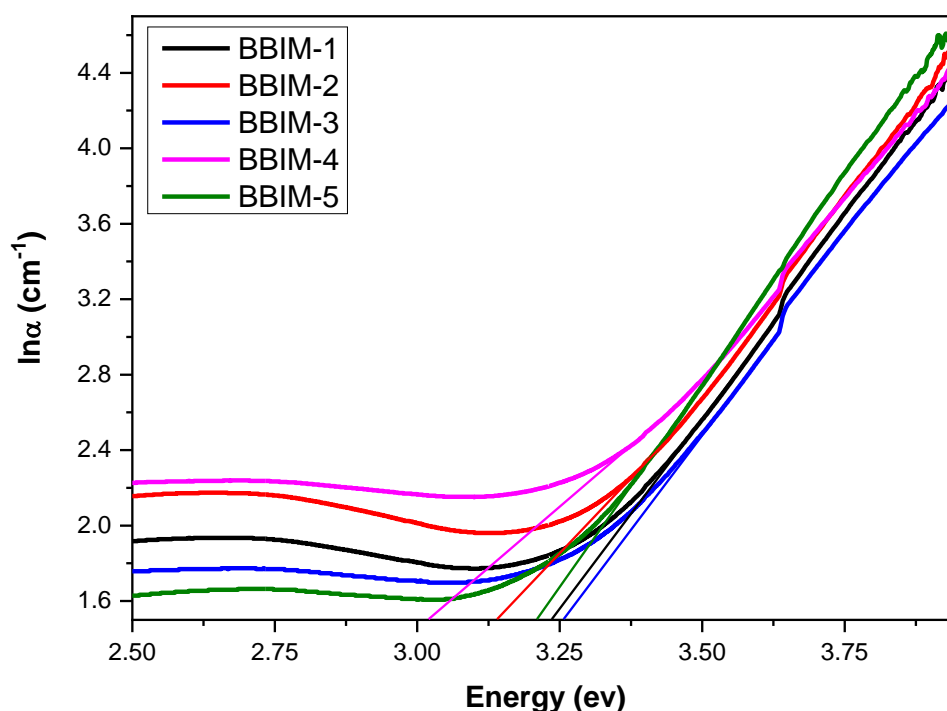
Fig. 4. Urbach curves of BBIM glasses.

The theoretical optical basicity *(Λ$_{th}$)* is estimated using the suggested relation by Duffy

$$\Lambda_{th} = (x_{In_2O_3} X \Lambda_{In_2O_3}) + (x_{BaO} X \Lambda_{BaO}) + (x_{B_2O_3} X \Lambda_{B_2O_3}) + (x_{CuO} X \Lambda_{Cuo}) \qquad (5)$$

Where $x_{In_2O_3}$, x_{BaO}, $x_{B_2O_3}$ and x_{CuO} are the mole % of the individual oxides and theoretical optical basicities of oxides $\Lambda_{In_2O_2}$, Λ_{BaO}, $\Lambda_{B_2O_3}$, and Λ_{Cuo} are taken from the literature [4] as $\Lambda_{In_2O_3} = 1.07$, $\Lambda_{BaO} = 1.23$, $\Lambda_{Cuo} = 1.11$ and $\Lambda_{B_2O_3} = 0.42$. The metallization parameter (M) is observed to decrease marginally decreased with In$_2$O$_3$ mole% in the glass. Materials showing larger metallization paraments near unity are typically insulators. The calculated M of the present glass samples are varying from 0.396 to 0.391, suggesting a semiconducting nature.

3.4. Electron Paramagnetic Resonance (EPR) spectra
        EPR is one of the most effective tools for obtaining useful data characterizing the glass structure, coordination of paramagnetic metal ions like Cu^{2+}, Mn^{2+} etc., and the covalency of glass components. Manganese with electronic configuration of [Ar] 3d^{5}4s^2, show +2, +3, +4, +6 and +7 oxidation states commonly. In which Mn^{2+} is more stable chemically and thermally [6]. Fig.5 displays a typical ESR spectrum of BBIM glass samples. All the present glasses doped with manganese ions displayed resonance signals at g =2.0, g =3.3 and g = 4.3. The electron paramagnetic spectra are analyzed using below given Spin-Hamiltonian [12,13]

$$H = B\beta.g.s + D(S_z^2 - s(s-1)/3] + I.A.S \qquad (6)$$

In the above equation the first term corresponds Zeeman interaction, second term gives zero field splitting and the last term represents hyperfine interactions. In general, Mn^{2+} ions show EPR resonance peaks at g≈3.3 and 4.3 corresponding to rhombic environment. The EPR peak for g≈2.0 arises when Mn^{2+} ions are distributed in octahedral symmetry.
The transition metal ions with d^5 configuration, gives rise to Kramer's doublets |±5/2›, |±3/2›, and |±1/2› with axial distortion of octahedral symmetry [14]. The spin degeneracy of the Kramer's doublets can be split by employing Zeeman field. The resonances are caused within the Kramer's doublets split by the Zeeman field because crystal field splitting is often significantly bigger than the Zeeman field. The EPR resonance peak at g = 2.0 is attributed to Mn^{2+} ion lying in octahedral symmetry surroundings. This transition happens between lower

doublets |±1/2›. The peaks corresponding to 3.3 and 4.3 are attributed to the rhombic environs of the Mn^{2+} ions and arise from the doublet |±3/2› [6,14].
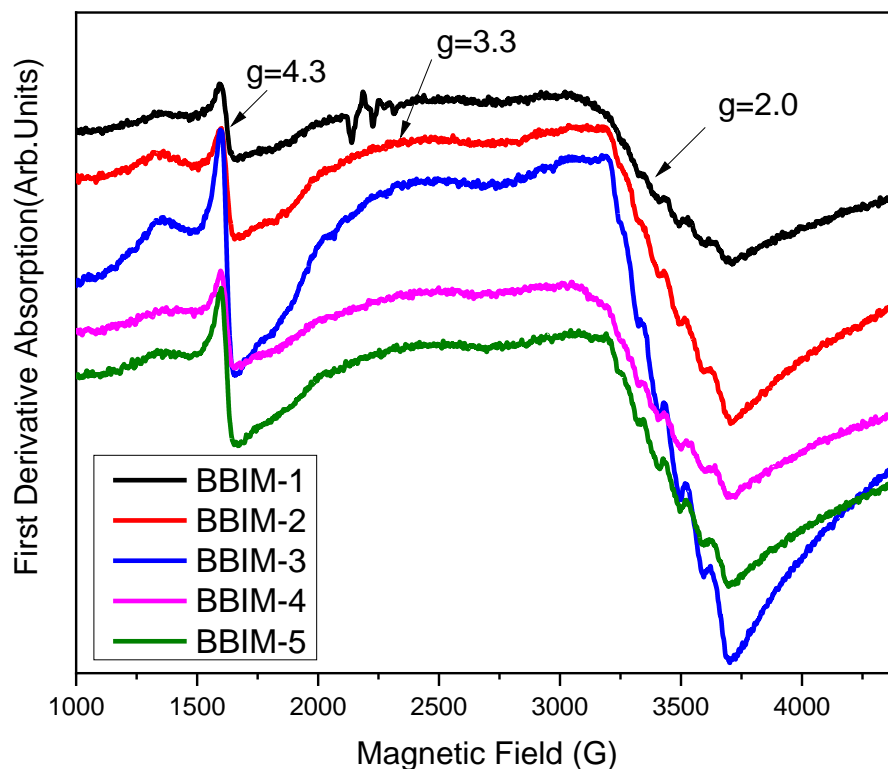
Fig. 5. EPR spectra of BBIM Glass samples.

All the present BBIM glasses clearly depicted a six-line hyperfine structure relating to the interaction of Mn^{2+} ion's electron spin having nuclear spin I (= 5/2) at g = 2.0. YThis transition is caused by exchange coupling of Mn^{2+} clusters and magnetic dipolar interaction. The intensity of EPR peak at g= 2.0 highly stronger than that of peak at g= 3.3 and 4.3 indicating presence of Mn^{2+} ions in octahedral environment rather than rhombic surroundings [15]. The resolution of hyperfine splitting (hfs) at g= 2.0 is a clue that Mn^{2+} ions are either dispersed in octahedral symmetric sites in isolation or considerably par apart from each other. The study indicates well defined symmetry of the manganese ion. The resolution of hfs sextet increased with increasing manganese ion concentration in the glass. This effect is because of broad distribution of either structural (spin-Hamiltonian) parameters or spin–spin interactions. The distortion in the crystalline field is evident from the line at g= 3.3 and the intensity of this peak diminished considerably with enhancing mole % in the glass network. The hyperfine peak at g= 4.3 has shown a decrement in its intensity at higher concentration of manganese ions.

It is known that splitting of hf depends on the electronegativity of the neighbors [16]. The hf splitting constant 'A'(= 87.0372×10^{-4} cm^{-1}) describes ionicity of bonding between Mn^{2+} ions and its ligands. The calculated 'A' values for the present glass systems indicated clearly ionic bonding environs between Mn^{2+} ions and the surrounding species. The magnitude of hfs constant A_{avg} are calculated from the expression having usual notation [17]:

$$A_{avg} = [(\Delta_{Opp} + \Delta_{Ott})/5 + (\Delta_{Mpp} + \Delta_{Mtt})/3 + (\Delta_{Ipp} + \Delta_{Itt})]/6 \qquad (7)$$

The g-value of hyperfine splitting expresses bonding character in the glass. If a negative shift is observed from free-electron g_e (=2.0023) value i.e (g_e-g), the bonding is ionic and for positive shift bonding is more covalent. In present study, calculated g-value is higher than the free electron g_e. Hence, shift in g being negative, it can be concluded that Mn^{2+} ion has ionic surroundings. The all samples have exhibited the same behaviour.

The zero-field splitting parameter (*D*) is estimated from the intensity of hyperfine lines using the ratio of allowed hyperfine lines obeying Δm=0 selection rule.

using the formula:

$$I_m \propto 2 - \frac{A^2(35-4m^2)}{2(g\beta H)^2} - \frac{5.334D^2}{(g\beta H)^2} - \frac{35.14D^2(35-4m^2)}{(g\beta H)^2} + \frac{208D^4(35-4m^2)^2}{(g\beta H)^4} \qquad (8)$$

In the above relation, *m* denotes nuclear spin magnetic quantum number, I_m *is* the intensity of allowed m^{th} hyperfine line, hyperfine splitting constant is 'A', and the remaining terms have their standard meanings. The present samples '*D*' values are noticed to be 25±0.30 mT and are similar to earlier reported values [5, 6]. It is

observed that 'D' values are not a function of composition in the present case which It suggests an insignificant divergence of crystal field strength at the locations of Mn^{2+} ion.

By comparing area under the EPR absorption curve of the samples with that of $CuSO_4.5H_2O$ standard reference, the no. of spins per unit volume (N) involved in the resonance are calculated using following expression proposed by Weil et al [18]:

$$N = \frac{A_x (Scan_x)^2 G_{std}(H_m)_{std}(g_{std})^2[s(s+1)]_{std}(P_{std})^{1/2}}{A_{std} (Scan_{std})^2 G_x(H_m)_x(g_x)^2[s(s+1)]_x(P_x)^{1/2}} * [std] \qquad (9)$$

The above terms have usual meaning. The paramagnetic susceptibility (χ) was estimated by using the following relation [19] with the standard notations.

$$\chi = \frac{Ng^2\beta^2 j(j+1)}{3K_BT} \qquad (10)$$
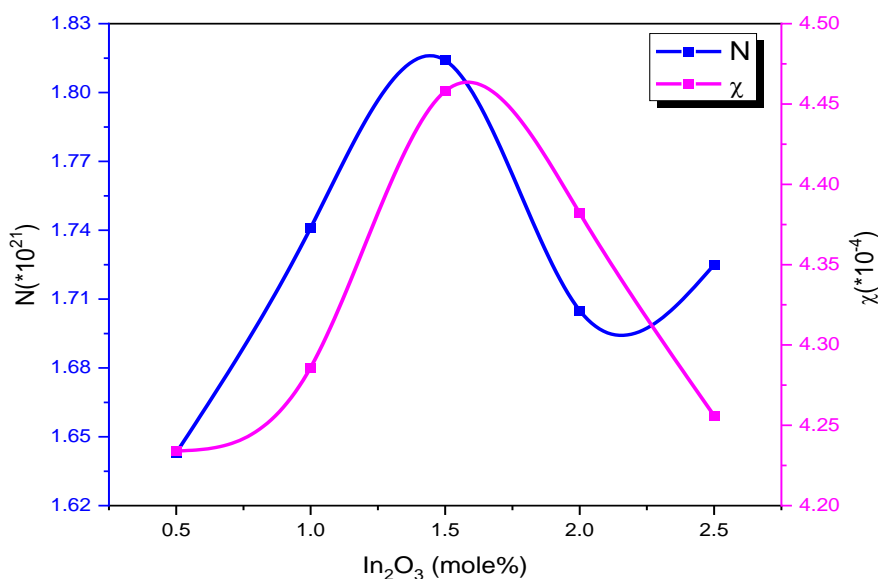
Fig. 6. Variation of N and χ with In_2O_3 concentration in BBIC glasses

Table 3: The g-value, shift in g-value (Δg), HF splitting constant (A), number of spins(N) and susceptibility (χ) of (30-x) BaO–69.5B_2O_3- xIn_2O_3:0.5MnO_2 glasses

Glass Code	$g_{2.0}$	Δg	A(10^{-4})cm^{-1}	D(mT)	N(10^{21})per Kg	χ(10^{-4})m^3/Kg
BBIM-1	2.063	-0.0609	85.292	26.55	1.643	4.234
BBIM-2	2.016	-0.0139	85.363	25.54	1.741	4.286
BBIM-3	2.015	-0.0123	89.588	25.73	1.814	4.458
BBIM-4	2.060	-0.0580	87.210	25.88	1.705	4.382
BBIM-5	2.019	-0.0167	87.733	25.37	1.725	4.256

Fig. 6. reveals variation of paramagnetic susceptibility(χ) and spin concentration (N) with In_2O_3 concentration. Both N and χ follow the same path and is nonlinear with In_2O_3 mole % indicating glass samples following a mixed oxide effect [20].

3.5. FTIR spectra

Borate groupings are categorized primarily into three regions: The 400-800cm^{-1} range corresponds to various borate groups bending modes and vibration of transition metal groups. The stretching of B-O in BO_4 produce vibrations of diborate to penta borate groups. The next zone spanning from 800 to 1200 cm^{-1} is seen. The third zone falls between 1200 and 1600 cm^{-1} and corresponds to stretching vibrations of several borate molecules in BO_3.
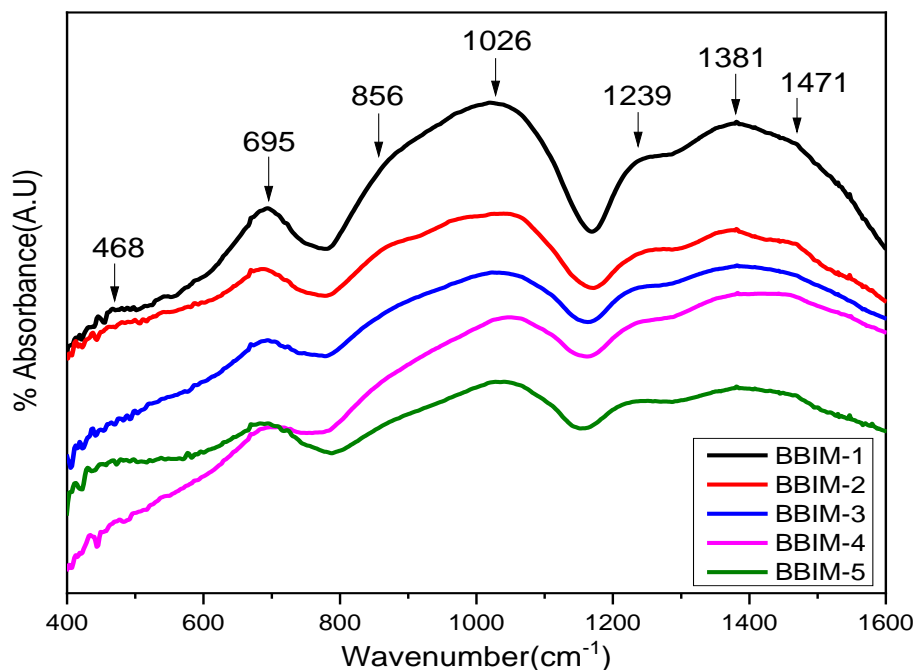
Fig. 7. FTIR spectra of BBIM glass system.

The infrared spectra are depicted in Fig.7. The exact band locations can be found out from the deconvoluted spectra (Fig.8). The residual graph is given in Fig. 10 Table.4 lists the placements of FTIR band assignments. In modified borate glasses, the above region of peaks slightly undergoes changes with composition of the glass changes. It is well known fact that composition of the glass able to modify or change the positions of infrared bands and peak resolutions. It noticed that the intensity of IR bands has undergone slight fluctuations with increasing In_2O_3 mole %. Barium borate glasses often include a small number of structural borate groups, such as tetrahedral units $[BO_4]$, boroxol, penta-, di-penta, di-borate, cyclic metaborate, and pyro-borate groups [20,21].
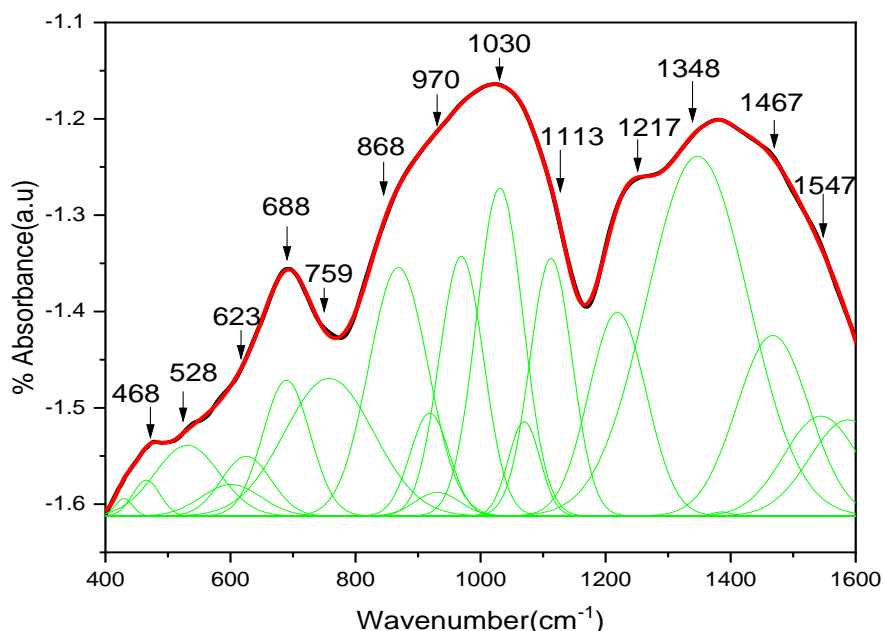
Fig.8. FTIR deconvolution plot for BBIM-1 glasses.

In the present work, owing to the heavy mass of indium atoms, the In–O stretching vibration modes are typically seen in the area of 800–300 cm^{-1} [22-24]. Spectra revealed a peak at 468 cm^{-1} due to Ba^{2+} metal cation vibrations, and vibrations due to In-O bonds [24]. The band at 695 cm^{-1} represents combined B-O-B in [BO$_3$] triangles and In-O [InO$_4$] bending vibrations. The identified 1026 cm^{-1} peak is a result of B–O symmetric bending mode of BO$_4$ units. The band located at 1239 cm^{-1} is appeared due to stretching vibrations of B–O bonds and B–O bridges between B$_3$O$_6$ and BO$_3$ triangles. The band observed at 1381 cm^{-1} owing to the B–O stretching vibrations of trigonal BO$_3$ units. At a wave number of 1471 cm^{-1}, stretching vibrations of trigonal BO$_3$ groups are seen.
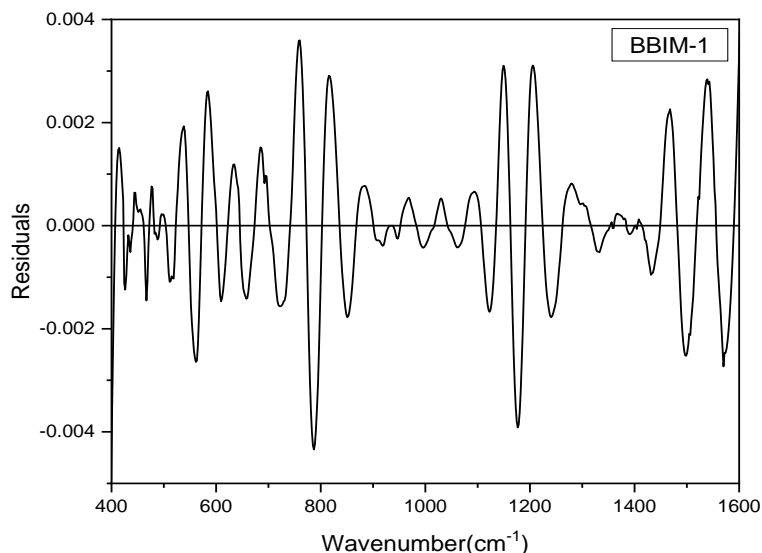
Fig. 9. Deconvolution residue graph of BBIM-1 glass.

The absorption bands in 800-1200 cm^{-1} region can be utilized to calculate percentage of BO$_4$ units (N$_4$) in glasses. The IR bands between 1200 and 1600 cm^{-1} are employed to determine the proportion of BO$_3$ units (N$_3$). N$_3$ and N$_4$ can be determined from the following formulae [21]:

$$N_3 = \frac{BO_3}{BO_3 + BO_4} \qquad \text{and} \qquad N_4 = \frac{BO_4}{BO_3 + BO_4} \qquad (11)$$

When the In$_2$O$_3$ concentration is raised by up to 2.0 mol%, the N$_3$ and N$_4$ values are observed to fall and rise in the present BBIC glasses, respectively indicating a reduction in the creation of BO$_3$ units and increase in generation of BO$_4$ units. Given that BO$_4$ units are denser than BO$_3$ units, it is possible to establish that the drop in BO$_3$ in present glasses is caused by an increase in BO$_4$ units as In$_2$O$_3$ concentration rises. the fluctuation of N$_3$ and N$_4$ values exhibits the exact opposite behaviour, as illustrated in Fig. 11.
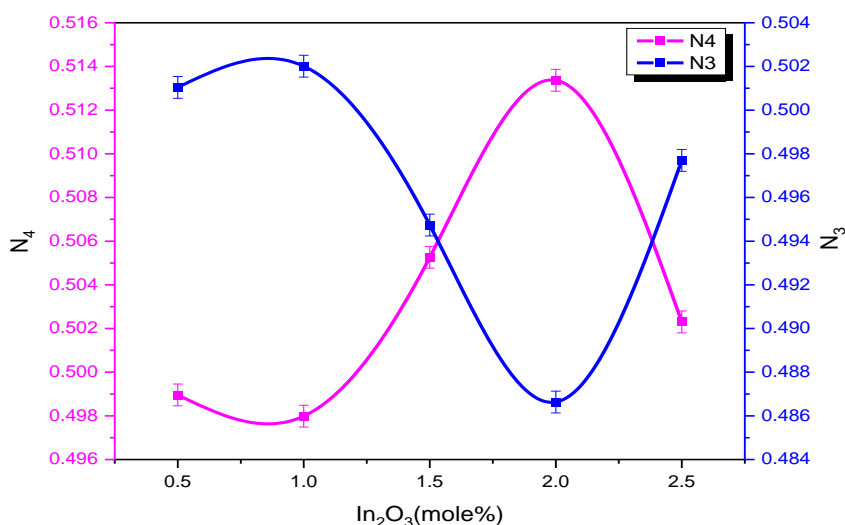
Fig. 10. Deviation of N$_3$ and N$_4$ values in BBIM glass samples.

Table.4 FTIR band positions and band allocation [12,25-29]

BBIM-1	BBIM-2	BBIM-3	BBIM-4	BBIM-5	Band assignment
468	436	434	434	431	Ba^{2+} metal cations vibration. InO_6 units and Mn-O (MnO_4) bond vibrations.
695	686	693	695	693	B–O–B bending vibration of $[BO_3]$ triangles and In–O bending vibration of $[lnO_4]$ tetrahedron.
856	863	871	868	878	BO_3-O-BO_4 bond-bending vibrations
1026	1039	1032	1049	1037	Symmetric Stretching vibration of B–O–B in $[BO_4]$ tetrahedron units.
1239	1255	1236	1234	1246	B–O stretching vibration of trigonal BO_3 units from meta-borate and ortho-borate group
1381	1381	1381	1381	1381	Stretching vibrations of B–O–B in
1471	1471	1467	1467	1469	$[BO_3]$ triangles

3.6 Raman spectra

Extensively, Raman spectroscopy is utilized to evaluate the structure of glass and investigate the functional groups that are likely present. Fig.11 depicts Raman spectra of BBIM glasses. Using Gaussian functions, the spectra of each BBIM glass sample were deconvoluted, allowing for a more accurate identification and assignment of all bands included in these spectra. Figures 12 and 13 depict, respectively, the deconvoluted Raman spectra and residue graph of the BBIM-1 glass sample. With the addition of In_2O_3, the variations in the glass structure of glasses may be comprehended in more detail. From the deconvolution spectra, the Raman bands cantered at 255 cm^{-1}, 350 cm^{-1}, 420 cm^{-1}, 560 cm^{-1}, 675 cm^{-1}, 760 cm^{-1}, 870 cm^{-1}, 970 cm^{-1}, 1080 cm^{-1},1185 cm^{-1},1305 cm^{-1},1440 cm^{-1}, 1550cm^{-1}, 1780 cm^{-1} and 1895 cm^{-1} can be observed in all the samples. Table. 5 provides the locations of the Raman bands. The centre peak locations show fluctuations due to change in composition.
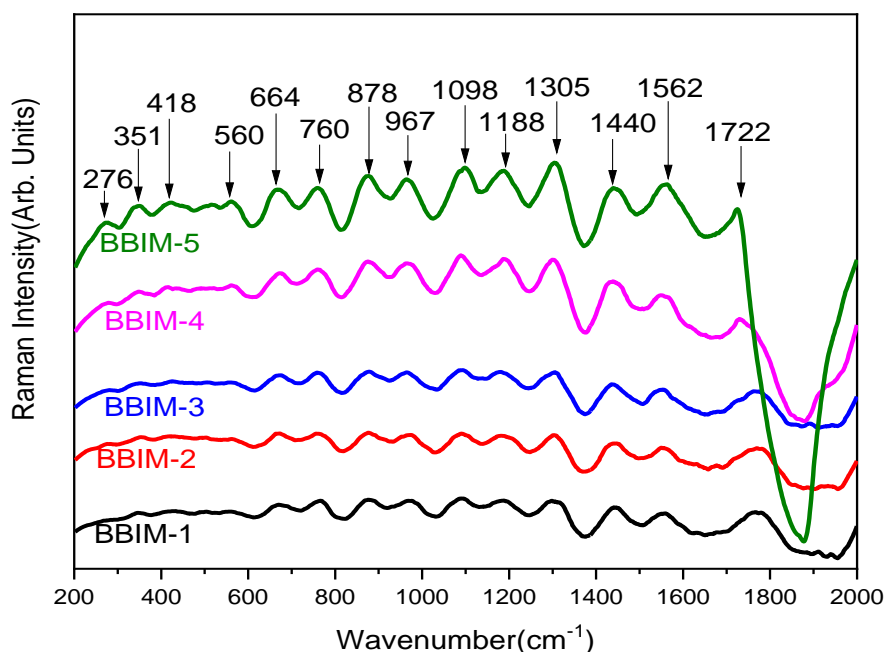
Fig.11 Raman spectra of BBIM glass systems.

Raman bands from 255 cm^{-1} to 675 cm^{-1} raised because of diborate groups and the vibrations of Ba^{2+} [30,31]. In this region bending and stretching vibrations In-O bonds are also included. [32]. A strong Raman band close to 1305 cm^{-1}, moved to towards low wavenumber side slightly which is ascribed to the symmetric breathing vibrations of BO_4 tetrahedra units with six-membered rings [30,33]. The addition of In_2O_3 in these glasses, Raman peaks are shifted to lower wavenumber. It can be assumed that conversion of boroxol rings tetraborate or tri-borates is not much stronger compared to their conversion into penta borate units. Raman bands at 870cm^{-1} & 1080cm^{-1} are due attributed to existence of penta-borates and di-borate groups respectively [26,30]. The band at 1722cm^{-1} is attributed to B–O$^{..}$ stretching in metaborate rings and chains [34,35]. The higher wavenumber modes are assigned to different types of O-H vibrations [32].
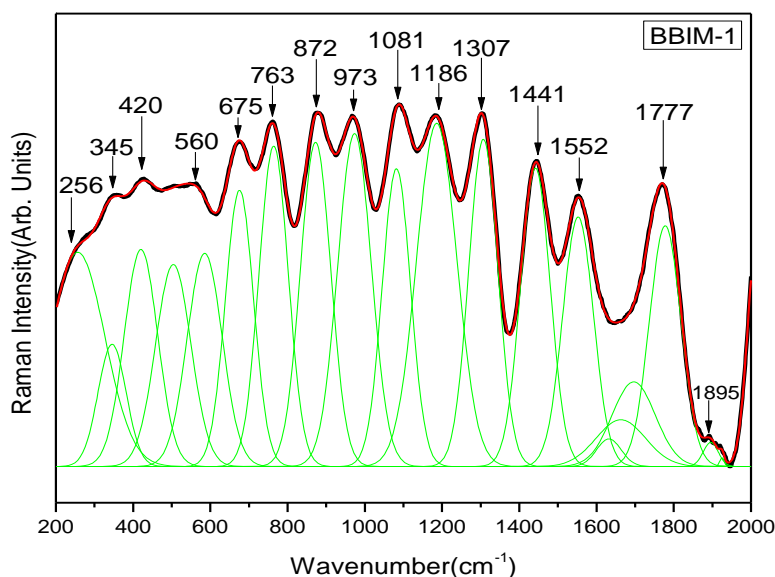
Fig. 12. Deconvoluted Raman spectra of BBIM-1 glass system.
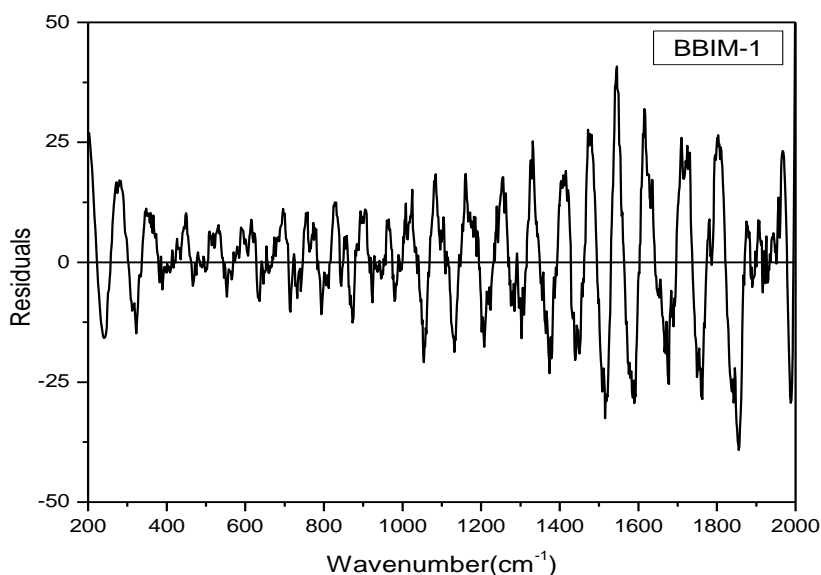
Fig. 13. Residue graph for the deconvoluted Raman spectra of BBIM-1 glass.

Table 5 Assignment of Raman bands present in the spectra [12,26.30,32,36-38]

Observe IR band positions	Band assignment
272-351	Ba and In metal cations vibrations
418-671	B–O–B linkage and In-O-B bending
760-764	BO_4 tetrahedra and lnO_4 units
963-971	B–O bond stretching of BO_4 units in tetraborate /orthoborate groups
1088-1092	BO_4 units
1098-1188	B–O⁻ stretching vibration in $[BO_3]$ trigonal with one or two BO_4 tetrahedra
1302-1398	BO_3 triangles vibrations in metaborate, pyroborate and ortho-borate units
1437-1444	B–O-vibrations of the BO_3 units attached to the large borate network
1558-1562	BO_3 triangles stretching vibrations of large borate network units.
1722-1768	Chain and ring type metaborate units

IV.   Conclusions

Mn-doped Indium borate glasses were synthesised by melting and quenching process. X-ray diffraction, UV-visible, EPR, FTIR and Raman spectroscopies were employed to examine prepared glass samples $(30-x)BaO-69.5B2O3-xIn_2O_3:0.5MnO_2$ (x= 0.5 to 2.5 mol%).

(a) The XRD patterns revealed amorphous characteristic of the glasses. The EPR spectra of Mn^{2+} ion containing present glasses exhibited strong sextet hyperfine splittings centered around $g \approx 2.0$ along with two weak resonance peaks at $g \approx 3.3$ and $g \approx 4.3$.

(b) Insignificant variation in 'A' and ''g values confirmed that these parameters are independent of Mn^{2+} ions concentration in the glass composition. From the values of A, it is concluded that the Mn^{2+} ion surroundings were ionic.

(c) The strong resonance EPR peak about $g \approx 2.0$, demonstrated a well-resolved hfs sextet in all glass samples. This is a strong indication that Mn^{2+} ions are distributed in isolation and are distorted octahedral sites. EPR peaks around $g \approx 3.3$ and $g \approx 4.3$ indicated that Mn^{2+} ions are located in the sites with rhombic symmetry. They are under the influence of strong crystal field effects.

(d) The optical absorption spectrum shows a broad band, and this has been attributed to Mn^{2+} ions in octahedral symmetry.

(e) FTIR and Raman spectroscopic analysis emphasized that the glass structure contains metal cation Ba^{2+}, InO_6 units, Mn-O (MnO_4), BO_3 triangles, BO_4 tetrahedra with metaborate, pyroborate and ortho-borate units.

Acknowledgements

References:

[1]. A. Ichoja, S. Hashim, S.K. Ghoshal, I.H. Hashim, S. A Dalhatu, R.S. Omar, Analysis of the physical, structural and optical characteristics of Dy3+-doped MgO–SrO–B_2O_3 glass systems, Indian Journal of Physics. 93 (2019) 1265–1273. https://doi.org/10.1007/s12648-019-01390-1.

[2]. A. Yahia, A. Attaf, H. Saidi, M. Dahnoun, C. Khelifi, A. Bouhdjer, A. Saadi, H. Ezzaouia, Structural, optical, morphological and electrical properties of indium oxide thin films prepared by sol gel spin coating process, Surfaces and Interfaces. 14 (2019) 158–165. https://doi.org/10.1016/j.surfin.2018.12.012.

[3]. P. Ramesh Babu, R. Vijay, V. Ravi Kumar, D. Krishna Rao, N. Veeraiah, The influence of In_2O_3 on electrical characteristics of iron mixed Li_2O–PbO–B_2O_3–SiO_2–Bi_2O_3 multi-component glass system, Ceram Int. 40 (2014) 8311–8322. https://doi.org/10.1016/j.ceramint.2014.01.036.

[4]. G. Sangeetha, K.C. Sekhar, A. Hameed, G. Ramadevudu, M.N. Chary, M. Shareefuddin, Influence of CaO on the structure of zinc sodium tetra borate glasses containing Cu^{2+} ions, J Non Cryst Solids. 563 (2021). https://doi.org/10.1016/j.jnoncrysol.2021.120784.

[5]. E.A. Davis, N.F. Mott, Conduction in non-crystalline systems V. Conductivity, optical absorption and photoconductivity in amorphous semiconductors, Philosophical Magazine. 22 (1970) 903–922. https://doi.org/10.1080/14786437008221061.

[6]. K.C. Sekhar, A. Hameed, G. Ramadevudu, M.N. Chary, M. Shareefuddin, Physical and spectroscopic studies on manganese ions in lead halo borate glasses, Modern Physics Letters B. 31 (2017). https://doi.org/10.1142/S0217984917501809.

[7]. S. Rajesham, K.C. Sekhar, Md. Shareefuddin, J.S. Kumar, Impact of MoO_3 on physical and spectroscopic (Optical, FTIR, Raman and EPR) studies of B_2O_3-CdO-Al_2O_3-ZnF_2 glasses for optical and shielding applications, Optik (Stuttg). (2022) 170241. https://doi.org/10.1016/j.ijleo.2022.170241.

[8]. V. Dimitrov, S. Sakka, Electronic oxide polarizability and optical basicity of simple oxides. I, J Appl Phys. 79 (1996) 1736–1740. https://doi.org/10.1063/1.360962.

[9]. J.A. Duffy, The electronic polarisability of oxygen in glass and the effect of composition, Journal of Non-Crystalline Solids, 297(2–3)(2002)275-284, https://doi.org/10.1016/S0022-3093(01)00940-1.

[10]. Dimitrov, Vesselin & Komatsu, Takayuki. Interionic Interactions, Electronic Polarizability and Optical Basicity of Oxide Glasses. Journal of the Ceramic Society of Japan. 108(2000)330-338. https://doi.org/10.2109/jcersj.108.1256_330.

[11]. M.R. Ahmed, M. Shareefuddin, EPR, optical, physical and structural studies of strontium alumino-borate glasses containing Cu^{2+} ions, SN Appl Sci. 1 (2019). https://doi.org/10.1007/s42452-019-0201-5.

[12]. M.R. Ahmed, B. Ashok, S.K. Ahmmad, A. Hameed, M.N. Chary, M. Shareefuddin, Infrared and Raman spectroscopic studies of Mn^{2+} ions doped in strontium alumino borate glasses: Describes the role of Al2O3, Spectrochim Acta A Mol Biomol Spectrosc. 210 (2019) 308–314. https://doi.org/10.1016/j.saa.2018.11.053.

[13]. G. Sangeetha, K. Chandra Sekhar, M. Narasimha Chary, M. Shareefuddin, Influence of magnesium oxide on the physical and spectroscopic properties of manganese doped sodium tetra borate glasses, Optik (Stuttg). 259 (2022). https://doi.org/10.1016/j.ijleo.2022.168952.

[14]. A. Abragam, B. Bleaney, Electron Paramagnetic Resonance of Transition Ions, 1970.

[15]. P. Giri Prakash, A. Murali, J.L. Rao, EPR and Optical Absorption Studies of Mn^{2+} ions in alkali borotellurite glasses, Modern Physics Letters B, 16(5-6) (2002)143-159, https://doi.org/10.1142/S0217984902003634.

[16]. J.S. Van Wieringen, Paramagnetic Resonance of Divalent Manganese Incorporated in Various Lattices, Discussions of the Faraday Society, 19(1955) 118, https://pubs.rsc.org/en/content/articlelanding/1955/df/df9551900118

[17]. K.C. Sekhar, A. Hameed, G. Ramadevudu, M.N. Chary, M. Shareefuddin, Physical and spectroscopic studies on manganese ions in lead halo borate glasses, Modern Physics Letters B. 31 (2017). https://doi.org/10.1142/S0217984917501809.

[18]. J.A. Weil, J.R. Bolton, Electron Paramagnetic Resonance: Elementary Theory and Practical Applications, Second Edition, 2006. https://doi.org/10.1002/9780470084984.

[19]. R.P. Sreekanth Chakradhar, A. Murali, J.L. Rao, Electron paramagnetic resonance and optical absorption studies of Cu ions in alkali barium borate glasses, Optical Materials, 109 (1998) https://doi.org/10.1016/S0925-3467(97)00167-5.

[20]. G. Sangeetha, K.C. Sekhar, A. Hameed, G. Ramadevudu, M.N. Chary, M. Shareefuddin, Influence of CaO on the structure of zinc sodium tetra borate glasses containing Cu^{2+} ions, J Non Cryst Solids. 563 (2021). https://doi.org/10.1016/j.jnoncrysol.2021.120784

[21]. Sangeetha, K. Chandra Sekhar, M. Narasimha Chary, M. Shareefuddin, Influence of magnesium oxide on the physical and spectroscopic properties of manganese doped sodium tetra borate glasses, Optik, 259 (2022) 168952. https://doi.org/10.1016/j.ijleo.2022.168952

[22]. M.I. Ivanovskaya, E.A. Ovodok, D.A. Kotsikau, Sol-gel synthesis and features of the structure of Au-In$_2$O$_3$ nanocomposites, Glass Physics and Chemistry. 37 (2011) 560–567. https://doi.org/10.1134/S1087659611050051

[23]. M. Jothibas, C. Manoharan, S. Johnson Jeyakumar, P. Praveen, Study on structural and optical behaviors of In$_2$O$_3$ nanocrystals as potential candidate for optoelectronic devices, Journal of Materials Science: Materials in Electronics. 26 (2015) 9600–9606. https://doi.org/10.1007/s10854-015-3623-x.

[24]. A. Yahia, A. Attaf, H. Saidi, M. Dahnoun, C. Khelifi, A. Bouhdjer, A. Saadi, H. Ezzaouia, Structural, optical, morphological and electrical properties of indium oxide thin films prepared by sol gel spin coating process, Surfaces and Interfaces. 14 (2019) 158–165. https://doi.org/10.1016/j.surfin.2018.12.012.

[25]. M.R. Ahmed, M.N. Chary, Md. Shareefuddin, Physical and structural studies of (30-x) BaO-xAl$_2$O$_3$ -69.5B$_2$O$_3$-0.5MnO$_2$ Glasses , Bulletin of Pure & Applied Sciences- Physics. 37d (2018) 146. https://doi.org/10.5958/2320-3218.2018.00020.9.

[26]. G. Padmaja, P. Kistaiah, Infrared and raman spectroscopic studies on alkali borate glasses: Evidence of mixed alkali effect, Journal of Physical Chemistry A. 113 (2009) 2397–2404. https://doi.org/10.1021/jp809318e.

[27]. V. Kumar, O.P. Pandey, K. Singh, Structural and optical properties of barium borosilicate glasses, Physica B Condens Matter. 405 (2010) 204–207. https://doi.org/10.1016/j.physb.2009.08.055.

[28]. Ardelean, Ioan I. and M. Todera. "FTIR structural investigation of 3B2O3·BaO glass matrix containing manganese ions." Journal of Optoelectronics and Advanced Materials 8 (2006)1118-1120, https://joam.inoe.ro/arhiva/pdf8_3/3Ardelean2.pdf

[29]. M.R. Ahmed, K.C. Sekhar, A. Hameed, M.N. Chary, M. Shareefuddin, Role of aluminum on the physical and spectroscopic properties of chromium-doped strontium alumino borate glasses, Int J Mod Phys B. 32 (2018). https://doi.org/10.1142/S0217979218500959.

[30]. A.K. Yadav, P. Singh, A review of the structures of oxide glasses by Raman spectroscopy, RSC Adv. 5 (2015). https://doi.org/10.1039/c5ra13043c.

[31]. J. Chandradass, D.S. Bae, K.H. Kim, A simple method to prepare indium oxide nanoparticles: Structural, microstructural and magnetic properties, Advanced Powder Technology. 22 (2011) 370–374. https://doi.org/10.1016/j.apt.2010.05.006.

[32]. D. Vitzthum, L. Bayarjargal, B. Winkler, H. Huppertz, Synthesis and Crystal Structure of the Acentric Indium Borate InB6O9(OH)3, Inorg Chem. 57 (2018) 5554–5559. https://doi.org/10.1021/acs.inorgchem.8b00518.

[33]. A.A. Alemi, H. Sedghi, A.R. Mirmohseni, V. Golsanamlu, Synthesis and characterization of cadmium doped lead-borate glasses, Bulletin of Materials Science. 29 (2006). https://doi.org/10.1007/BF02709356.

[34]. B.N. Meera, A.K. Sood, N. Chandrabhas, J. Ramakrishna, Raman study of lead borate glasses, 1990.

[35]. K.C. Sekhar, A. Hameed, V.G. Sathe, M.N. Chary, M.D. Shareefuddin, Physical, optical and structural studies of copper-doped lead oxychloro borate glasses, Bulletin of Materials Science. 41 (2018). https://doi.org/10.1007/s12034-018-1604-4.

[36]. Samdani, Md. Shareefuddin, G. Ramadevudu, S.L.S. Rao, M. Narasimha Chary, Physical, Optical, and Spectroscopic Studies on MgO-BaO-B$_2$O$_3$ Glasses , ISRN Ceramics. 2013 (2013) 1–11. https://doi.org/10.1155/2013/419183.

[37]. K. Nanda, N. Berwal, R.S. Kundu, R. Punia, N. Kishore, Effect of doping of Nd3+ ions in BaO–TeO$_2$–B$_2$O$_3$ glasses: A vibrational and optical study, J Mol Struct. 1088 (2015) 147–154. https://doi.org/10.1016/j.molstruc.2015.02.021.

[38]. C.R. Gautam, A.K. Yadav, Synthesis and Optical Investigations on (Ba,Sr)TiO: TiO$_3$ Borosilicate Glasses Doped with La$_2$O$_3$, Optics and Photonics Journal, 03(2013)1–7. https://doi.org/10.4236/opj.2013.34a001.